Preparation and Characterization of Fe^{3+}, La^{3+} Co-Doped Tio_2 Nanofibers and Its Photocatalytic Activity

Ning Wu, Ph.D., Li Chen, Ph.D., Yanan Jiao, Ph.D., Guangwei Chen, Jialu Li

Tianjin Polytechnic University, Tianjin CHINA

Correspondence to:
Ning Wu email: wuning@tjpu.edu.cn

ABSTRACT

Nanofibers of Fe^{3+}, La^{3+} co-doped titanium dioxide (TiO_2)/Polyvinyl acetate (PVAc) composite have been prepared by electrospinning process. The ceramic nanofibers co-doped with metal ions were obtained by high temperature calcination of the organic/inorganic composite fibers. The structure, crystalline state and surface morphologies were characterized by scanning electron microscopy (SEM), X-ray Diffraction (XRD), Fourier transform infrared spectroscopy (FTIR) and atomic force microscope (AFM), respectively. The observation by SEM revealed that there was a significant difference in the fibrous structure of the nanofibers before and after co-doping and calcinating. XRD patterns indicated the lattice of TiO_2 nanocrystalline were distorted by co-doped ions. FTIR spectrum further confirmed the presence of Fe and La oxidate in the co-doped nanofibers. AFM images showed that comparing to TiO_2 nanofibers, the roughness was increased on the surface of co-doped nanofibers. Before and after doping, the photocatalysis activity of the nanofibers were analyzed using ultraviolet-visible spectrophotometer (UV-Vis). The photocatalysis activity were significantly improved by the porous roughness surface structure and cooperative actions of Fe^{3+}, La^{3+} co-doping .

Keywords: Fe^{3+}, La^{3+} co-doped TiO_2; Electrospinning; Nanofiber; Photocatalysis activity

INTRODUCTION

Titanium dioxide (TiO_2) has been regarded as an important semiconductor material because of its wide applications related to catalytic devices, gas sensors, batteries and solar cells [1-4], mostly attributed to its low cost and special optical and electronic properties [5]. However, the big band-gap and fast charge-carrier recombination have proved to strongly limit the photocatalytic activity of TiO_2. Some recent studies related to photocatalytic activity show doping two metal or nonmetal components into anatase TiO_2 lattice is a very effective way for improving the photocatalytic activity of TiO2 [6-8].

Besides the doping method, TiO_2 with porous structure possesses more reactive activity dots and also favors of reactants adsorption and product desorption [9], both of them beneficial to the improvement of photocatalysis efficiency. Nanofibrous network structure has very small pore size and very high porosity [10]. In order to obtain nanofiber structure materials, various preparation methods have been developed [11–14]. Among many available methods for producing nanofibers, the electrospinning is a very convenient and versatile method for fabricating continuous nanofibers with uniform diameters from various polymers, ceramics and composites [15–17].

In the present work, TiO_2 co-doped with Fe^{3+} and La^{3+} in the form of nanofibers were prepared by combining sol-gel method, electrospinning technology and calcination process. The fibrous structure, components, crystallize state and surface morphology of Fe^{3+}, La^{3+} co-doped TiO_2 nanofibers were investigated by scanning electron microscope (SEM), Fourier Transform Infrared Spectroscopy (FTIR), X-ray Diffraction (XRD) and atomic force microscope (AFM).The photocatalysis efficiency for the methylene blue degradation under ultraviolet-visible irradiation was compared between un-doped and co-doped nanofibers . The mechanism of two dopants on the improvement of TiO_2 nanofiber photocatalysis activity was discussed.

EXPERIMENTAL

Synthesis of Co-Doped Tio_2 Nanofibers

All reagents used in the experiments were of analytical grade without further purification. $Ti(OC_4H_9)_4$ solution was used as molecular precursor

of TiO_2. In order to control the reaction kinetics, acetylacetone was acted as a coupling agent to moderate the reaction rate. 5mL acetylacetone and 0.03mol $Ti(OC_4H_9)_4$ were added into 10mL anhydrous ethanol with stirring(Solution A). The preparation of Solution B is by adding a given amount of $Fe(NO_3)_3 \cdot 9H_2O$ and $La(NO_3)_3 \cdot 6(H_2O)$ into the solution of 5mL deionized water and 5mL ethanol. Then, Solution B was added dropwise into Solution A with vigorous stirring for 5h at room temperature. After being mixed uniformly, stable, wheat Fe^{3+}, La^{3+} co-doped TiO_2 sol was obtained (Solution C). PVAc solution with a concentration of 15wt % (Solution D) was also prepared by dissolving the PVAc particles in acetone. Solution C was mixed with Solution D in a 1:1 ratio by stirring for 6 h, to obtain the Fe^{3+}, La^{3+} co-doped PVAc/TiO_2 composite solution. The composite solution is placed in a syringe for electrospinning. A high voltage (20KV) was applied to the spinning solution via an alligator clip attached to the syringe needle. The solution was delivered to a blunt needle (the nozzle diameter was about 0.7mm) via a microinfusion pump (WZ-50C2, Zhejiang, China) to control the solution flow rate at 1.0ml/h. The electrospun fibers were collected on a sheet glass. The as-prepared composite fibers were subjected to 500℃ calcination for 2h to obtain Fe^{3+}, La^{3+} co-doped TiO_2 nanofibers. For convenience, the samples were labeled as P/T for PVAc/TiO_2, TFL for Fe^{3+} and La^{3+} co-doped TiO_2, and P/TFL for Fe^{3+} and La^{3+} co-doped PVAc/TiO_2.

Characterization

The fibrous structures of the nanofibers were observed with SEM (HITACHI S-4800) after gold coating. XRD patterns of all samples were obtained at room temperature with a BRUKER D8 diffractometer (Cu Kα radiation, λ = 1.5406 A°) with the scanning rate of 5°/min. FTIR of the samples were recorded on Nicolet Nexus ATR-FTIR at a scanning rate of 64 s^{-1}. The AFM scanning was performed on a CSPM4000 AFM (Benyuan, China), with a scanning frequency of 1.0 Hz in tapping mode.

Measurement of Photocatalytic Efficiency

The photoreaction was conducted in a 200mL cylindrical vessel with a water-cooled quartz jacket. Irradiation was provided by a 150W tungsten halogen lamp and an 8W UV lamp, located in the center of the quartz jacket. A magnetic stirrer was equipped at the bottom of the reactor to achieve effective dispersion. Air was bubbled through the reaction solution from the bottom to ensure a constant dissolved O_2 concentration. The photocatalytic activity of co-doped TiO_2, pure TiO_2 nanofibers was also tested. The amount of nanofibers chosen was 0.2 g/L, the methylene blue concentration was 1.5×10^{-5}mol/L, and 100mL methylene blue solution was used for each photocatalytic degradation study. The temperature of the reaction solution was maintained at 25±0.5 ℃. The reactor was placed in a darkroom first until it reaches adsorption equilibrium. A certain amount of reactive solution was withdrawn at 30 min intervals. The residual concentration of methylene blue was measured at 665 nm wavelength with a 721 UV-Vis spectrophotometer (Jingke, China).

RESULTS AND DISCUSSION

Fibrous Structure

The SEM images of electrospun P/T nanofiber and P/TFL composite nanofibers before calcinations are illustrated in *Figure 1*. The nanofibers are randomly distributed on the collector to form a 3-D fibrous web. The morphology and diameters of the electrospun P/TFL composite nanofibers are significantly affected by the Fe^{3+} and La^{3+} added. As can be seen from *Figure 1*, some discontinuous dots appeared on the surface of P/TFL nanofibers, possibly because some exposed Fe^{3+} and La^{3+} ions were oxidized by air. It can also be observed from *Figure 1* that compared to P/T nanofibers, the average diameter of P/TFL nanofibers increased with Fe^{3+} and La^{3+} loading. *Figure 2* displays the SEM images of 500℃ calcined TiO_2 nanofibers and TFL nanofibers. It is observed from *Figure 2* that the fibrous structure of TiO_2 nanofibers and TFL nanofibers are well reserved after 500℃ calcinations. It can also be found from *Figure 2* that compared to TiO_2 nanofibers, the TFL nanofibers clearly exhibit a bend fibrous web and porous structure. The doping of Fe^{3+} and La^{3+} favors the porous fibrous structure formation.

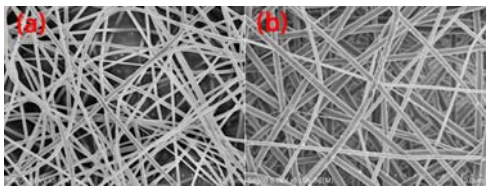

FIGURE 1. SEM images of (a) P/T nanofibers and (b) P/TFL composite nanofibers.

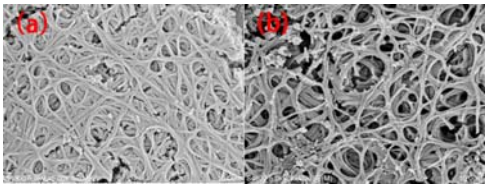

FIGURE 2. SEM images of (a) TiO_2 nanofibers and (b) TFL nanofibers calcinated at 500℃.

XRD Analysis

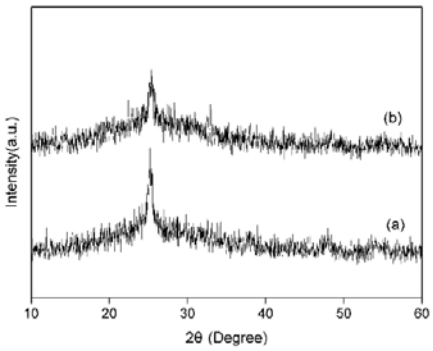

FIGURE 3. XRD patterns of (a)TiO_2 nanofibers and (b)TFL nanofibers.

The XRD patterns of TiO_2 and TFL nanofibers calcined at 500℃ are shown in *Figure 3. Figure 3(a)* shows a series of peaks at 2θ= 25.3°, 37.8°, 48.0° and 55.1°, corresponding to those of pure anatase TiO_2 (JCPDS 21-1272). *Figure 3(b)* also reveals some crystalline peaks in the same degrees but the intensities are weaker. This indicates that co-doping influenced the crystallinity of TiO_2 nanofibers. The radii of Ti^{4+}, Fe^{3+}, and La^{3+} for hexa-coordinate are 69, 74.5, and 115pm, respectively. According to Pauling's principle, Fe^{3+} ions can merge with the matrix of the TiO_2 nanoparticles without causing much crystalline distortion. Due to the large difference on the ionic radius between Ti^{4+} and La^{3+}, it is difficult for La^{3+} ions to substitute Ti^{4+} ions, and therefore most of the La^{3+} ions are distributed on the surface of the matrix of TiO_2 nanoparticles. However, the substitution of some La^{3+} ions into the matrix of TiO_2 will seriously affect the hexa-coordinate and distort the matrix [18].

FTIR Analysis

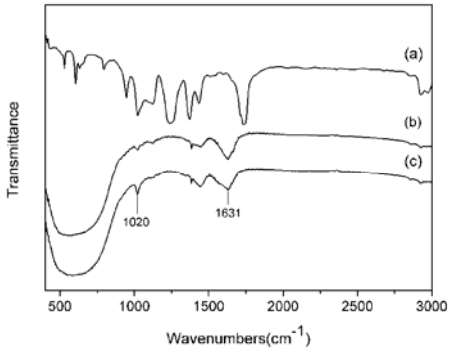

FIGURE 4. FTIR spectra of (a) P/TFL nanofibers, (b) TiO_2 nanofibers, and (c) TFL nanofibers.

The formation of metal oxide nanofiber is further supported by FTIR analysis *Figure 4. Figure 4* presents the FTIR spectra of the P/TFL nanofiber (Spectrum a), the TiO_2 nanofiber (Spectrum b), and the TFL nanofiber (Spectrum c) nanofiber in wave numbers ranging from 400 to 3000 cm^{-1}.Specturm a reveals strong absorption bands between 800 and 1800cm^{-1} which can be assigned to bending and stretching frequencies of the PVAc, whereas the absorption peaks of inorganic components in the P/TFL system are not obvious. After calcinations at 500℃, from spectrum b and c, all these strong features are removed. No sign of absorbed water or hydroxyl or hydrocarbon impurity can be observed. Instead, there is a wide band from 470 to 750 cm^{-1}, due to the formation of TiO_2 crystallization. Compared to spectrum b, the characteristic peaks of La_2O_3 at 1020 cm^{-1} appeared in Spectrum c, and the absorption band from 1500 to 1631cm^{-1} becomes gently in Spectrum c. The characteristic peaks of Fe_2O_3 also appeared in this area (from standard diagram database).

Surface Morphology

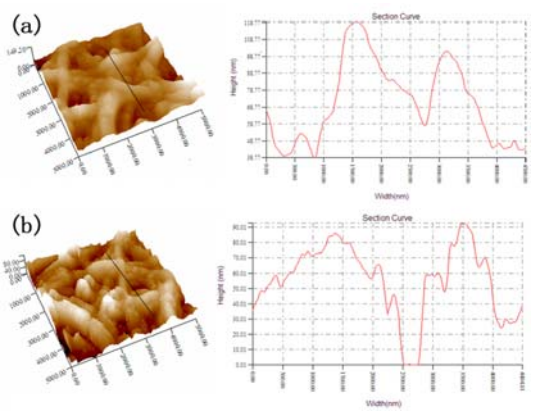

FIGURE 5. AFM images and section curves of (a) TiO_2 nanofibers, (b) TFL nanofibers

The surface morphology of electrospun nanofibers before and after doping is investigated by AFM. The AFM images and cross section curves of TiO_2 nanofibers and TFL nanofibers are presented in *Figure 5.* Images in *Figure 5* reveal that the nanofibers are randomly oriented in the web, with some nanoparticles forming aggregation structures on the surface of both TiO_2 and TFL nanofibers. According to the AFM images and cross section curves, the surface roughness of nanofibers is increased after co-doping of Fe^{3+} and La^{3+}. This is possibly attributed to some Fe^{3+} and La^{3+} oxides deposited on the surface of TFL nanofibers. It can also be observed in *Figure 5(b)* that some deep holes exist among the TFL nanofibers.

Photocatalytic Activity

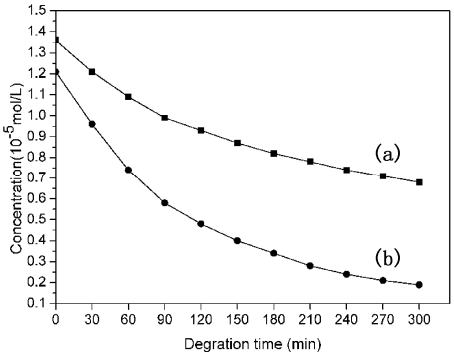

FIGURE 6. Degradation curves of methylene blue with irradiation time. (a)TiO_2 nanofibers,(b) TFL nanofibers.

The concentration variations of methylene blue with irradiation time are presented in *Figure 6*. When the two reaction solution systems reach adsorption equilibrium, the starting concentration of methylene blue in TFL nanofibers solution system is less than TiO_2's, which imply in comparison with pure TiO_2 nanofibers, TFL nanofibers possess better adsorption ability. Fe^{3+} and La^{3+}co-doping can significantly enhance the photocatalytic activity compared with un-doped TiO_2 nanofibers. Such an improvement caused by co-doping of Fe^{3+} and La^{3+}leads to the variation of micro morphology and lattice structure of TiO_2 nanofibers. The TFL nanofibers have clearer porous structure and rougher surface morphology *(Figure 2, Figure 5),* which amplified the contact areas among reactants and photo catalysts. A larger specific surface area favors reactants adsorption and products desorption, which accelerated the photocatalysis rate of TiO_2 nanofibers. XRD analysis *(Figure3*) indicates that Fe^{3+} ions are easily entered into the TiO_2 lattice and substitute the Ti^{4+}. Since the energy level of Fe^{3+} is close to the conduction band and valence band of TiO_2, the recombination of the photoexcited charge carriers in the nanostructure is retarded by Fe^{3+}, which can act as both an electron trap and a hole trap [19, 20]. Owing to the large difference of radii between La^{3+} and Ti^{4+}, the doping of La^{3+} induced the lattice distortion and expansion in the crystal matrix. The expansion generates shallow energy states in the bottom of the conduction band and served as electron trap site in nanocrystalline TiO_2. Since the trapped electrons will quickly recombine with their mobile counterparts, nanocrystalline TiO2 doped with Fe^{3+} or La^{3+} alone can hardly improve the separation of charge carriers and interfacial charge transfer simultaneously. When Fe^{3+} and La^{3+} are co-doped into the nanocrystalline TiO_2, Fe^{3+} may mainly serve as a hole trap and La^{3+} as an electron trap. The recombination of the charge carriers is restrained by such cooperative operations.

CONCLUSIONS

Fe^{3+}, La^{3+} co-doped PVAc/TiO_2 composite nanofibers were fabricated by combining the sol–gel process and the electrospinning technique. The composite nanofibers were calcined in air at 500℃ to obtain Fe^{3+}, La^{3+} co-doped TiO_2 nanofibers. SEM images revealed a fibrous porous structure of Fe^{3+}, La^{3+} co-doped TiO_2 nanofibers. From the FTIR and XRD analysis, it can be concluded that Fe^{3+}, La^{3+} co-doping leads to an increase in electron and hole

traps and the distortion of TiO_2 lattice. It was also found from an AFM images and section curves that the co-doped TiO_2 nanofiber mats possess deep holes and a rough surface. The photocatalysis activity of Fe^{3+} and La^{3+} co-doped TiO_2 nanofibers are significantly improved due to the porous surface structure and the cooperative actions of the two dopants.

ACKNOWLEDGEMENT

The research work was financial supported by the National Natural Science Foundation of China (NO.11072175) and Program of Tianjin Science & Technology Planning Project (NO.11ZCKFSF00500)

REFEARENCES

[1] Dong W.;Cogbill A.; Zhang T.; Ghosh S.; Tian ZR.; *J. Phys. Chem. B* 2006, 110, 16819 - 16822.

[2] Ruiz A.M.; Sakai G.; Cornet A.; Shimanoe K.; Morante J.R.; Yamazoe N.; *Sens. Actuators, B* 2003,93,509-518.

[3] Choi M.G.; Lee Y.G.; Song S.W.; Kim K.M.; *Electrochim. Acta.,* 2010, 55, 5975-5983.

[4] Lee C.Y.; Hupp J.T.; *Langmuir* 2010, 26, 3760-3765.

[5] Zhang L.; Kanki T.; Sano N.; Toyoda A.; *Sep. Purif. Technol.* 2003, 31,105-110.

[6] Yu H.F.; Yang S.T.; *J. Alloys. Compd.* 2010,492, 695-700

[7] Shen Y.; Xiong T.; Li T.; *Appl. Catal, B* 2008, 83,177-185.

[8] Shi J.W.; Zheng J.T.; Hu Y.; Zhao Y.C.; *Mater. Chem. Phys.* 2007,106, 247-249.

[9] Wang X.; Yu J.C.; Ho C.; *Langmuir,* 2005, 21, 2552-2559.

[10] Subbiah T.; Bhat G.S.; Tock R.W.; Parameswaran S.; Ramkumar S.S.; *J. Appli. Polym. Sci.* 2005, 96, 557-569.

[11] Zhang S.; Gelain F.; Zhao X.; *Semin. Cancer. Biol.,* 2005, 15, 413-420.

[12] Nain A.S.; Wong J.C.; Amon C.; Sitti M.; *Appl. Phys. Lett.* 2006, 89, 183105 - 183107.

[13] Mark J.P.; Larry G.S.; *Chem. Mater.* 2000,12,280-283.

[14] Bal S.; *Mater. Des.* 2010, 31, 2406-2013.

[15] Yeo L.Y.; Friend J.R.; *J. Exp. Nanosci.,* 2006,1,177-181.

[16] Zhang Y.; Li J.; Li Q.; Zhu L.; Liu X.; *J. Colloid. Interface. Sci.* 2007, 307, 567 - 570.

[17] Kim C.W.; Kim D.S.; Kang S.Y.; Marquez M.; Joo Y.L.; *Polymer* 2006, 47, 5097-5107.

[18] Jing L.; Sun X.; Xin B.; Wang B.; Cai W.; *J. Solid State. Chem.* 2004,177, 3375-3382.

[19] Choi W.; Termin A.; Hoffmann M.R.; *J. Phys. Chem.* 1994, 98, 13669-13679.

[20] Kim D.H.; Hong H.S.; Kim S.J.; *J. Alloys Compd.* 2004, *375*,259-2.

AUTHORS' ADDRESSES

Ning Wu, Ph.D.
Li Chen, Ph.D.
Yanan Jiao, Ph.D.
Guangwei Chen
Jialu Li
Tianjin Polytechnic University
Hedong District
Chenglin Avenue No.63
Tianjin 300160
CHINA